ACS NANO

www.acsnano.org

ARTICLE

Self-Assembly of Bolaamphiphiles into 2D Nanosheets *via* Synergistic and Meticulous Tailoring of Multiple Noncovalent Interactions

Zili Li and Zhiqun Lin*

Cite This: *ACS Nano* 2021, 15, 3152–3160

Read Online

ACCESS | Metrics & More | Article Recommendations | Supporting Information

ABSTRACT: A bolaamphiphile possessing a hydrophobic skeleton and two hydrophilic groups at both ends represents an important class of building blocks toward a rich variety of self-assembled materials for use in ion transport, optoelectronic devices, and drug and gene delivery. Herein, we report a *one-step* synthesis of an array of rationally designed anionic bolaamphiphiles and unravel the correlation between molecular structure of anionic bolaamphiphiles and their disparate self-assemblies *via* synergistic and meticulous tailoring of a set of interactions. Intriguingly, by delicately regulating the interactions among these supramolecular interactions, two-dimensional (2D) nanosheets are crafted *via* self-assembly of anionic bolaamphiphiles. Particularly, single-layered 2D nanosheets are formed through the synergy of aromatic $\pi-\pi$ stacking, hydrophobic, hydrogen-bonding, and electrostatic repulsion interactions. In contrast, the selective converting of anionic headgroups of bolaamphiphiles into nonpolar alkyl chain screens the electrostatic repulsion between neighboring bolaamphiphiles while keeping the other segments of bolaamphiphiles intact, thereby allowing them to self-assemble into multilayered 2D nanosheets. Interestingly, the intrinsically charged 2D nanosheets could anchor oppositely charged metal nanoparticles *via* electrostatic attraction. Conceptually, anionic bolaamphiphile-derived 2D nanosheets may function as a substrate to position a diversity of nanocrystals and conjugated polymers for a broad range of applications in catalysis, optical devices, and photothermal therapy.

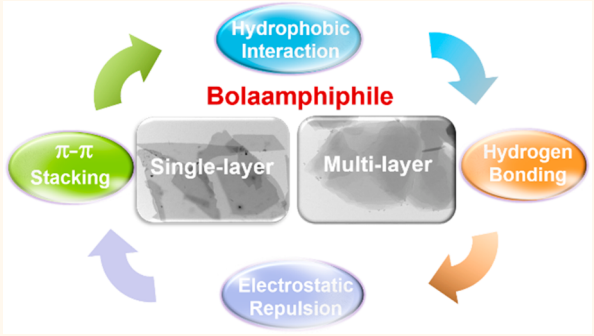

KEYWORDS: *bolaamphiphile, self-assembly, single-layered nanosheets, multilayered nanosheets, multiple noncovalent interactions*

INTRODUCTION

Two-dimensional self-assembled architectures composed of organic building blocks have garnered much attention due to their low density, good ductility, and more importantly the ability to precisely control their compositions, structures, and functionalities.[1−6] They find promising applications in electronics,[7] catalysis,[8] drug delivery,[9] and membranes for separation and filtration.[10] Despite the advantageous attributes noted above, much attention has been centered on the synthesis of sheet-like organic nanomaterials. However, their formation mechanism and functionalization have yet to be largely explored. Furthermore, it remains challenging to access free-standing single-layered 2D organic nanosheets. Two-dimensional organic nanosheets can be achieved by either top-down[11−13] or bottom-up[4,14−23] approaches. In spite of its simplicity, the top-down approach is time-consuming with low yield and often invokes the use of solvents[24] or mechanical forces[25] to exfoliate nanosheets from the layered host compounds. As a result, the defects on nanosheets are inevitable during delamination, and the size of exfoliated nanosheets is extremely small and difficult to control. In contrast, the bottom-up route involves the self-assembly of polymers[4,14,16,17] or small molecules[18−23] as building blocks into 2D organic nanosheets under mild synthetic conditions. Self-assembly is a convenient, energy- and resource-saving form to produce nanosheets with a molecular-level precision.[26,27] In this strategy, the size and morphology of the resulting 2D assemblies can be readily tailored by controlling the time[15] and location[16] of the self-assembly process. Moreover, such a bottom-up, solution-based self-assembly

Received: November 18, 2020
Accepted: January 25, 2021
Published: January 28, 2021

https://dx.doi.org/10.1021/acsnano.0c09693
ACS Nano 2021, 15, 3152–3160

process can achieve dimensional control, create segmented assemblies, easily introduce functional moieties into the resulting architectures, and yield large-area nanosheets. Clearly, it is highly desirable to develop a facile molecular design strategy for preparing 2D organic nanosheets with diverse compositions, structures, and functionalities.

To date, organic 2D nanosheets with a lateral size of a few hundred nanometers to several microns have been produced *via* self-assembly of small molecules driven by various noncovalent interactions ($\pi-\pi$ stacking, multiple hydrogen bonds, metal coordination, and charge transfer interactions).[28−30] It is notable that the single-layer nanosheet is highly unstable and tends to form multilayer nanosheets to lower the overall surface energy. Thus, an additional exfoliation step is often needed to convert multilayered nanosheets into single-layered nanosheets. In this context, significant efforts have been devoted to developing reliable and applicable routes to free-standing single-layered 2D nanosheets. Recently, bolaamphiphiles containing a hydrophobic skeleton with a hydrophilic group at each end have emerged as appealing small molecules to achieve diverse assemblies with distinct structures for use in ion transport, optoelectronics, and drug and gene delivery.[28,29,31−34] Despite some impressive studies on 2D organic multilayered nanosheets *via* self-assembly of bolaamphiphiles,[20−22,35] the attempts to interrogate the relation between the structures of bolaamphiphiles and the formed 2D sheet-like self-assemblies for precisely engineering 2D nanosheets have been comparatively few and limited in scope. Moreover, the ability to design bolaamphiphiles with different molecular structures may enable further investigation into the structure−property relationship of 2D nanosheets and inspire their potential applications.

Herein, we develop a robust strategy for crafting 2D organic nanosheets *via* self-assembly of a suite of *rationally designed* and *one-step-synthesized* anionic bolaamphiphiles, and more importantly unveil the correlation of the molecular structure of bolaamphiphiles and the resulting 2D nanosheets, enabled by synergistically and judiciously tailoring a series of noncovalent interactions among bolaamphiphiles. First, the originally carboxylic acid-terminated bolaamphiphiles are converted into anionic bolaamphiphiles in the presence of tetramethylguanidine. The synergy of four strong noncovalent interactions, that is, aromatic $\pi-\pi$ stacking, hydrogen-bonding, hydrophobic, and electrostatic repulsion interactions, drives anionic bolaamphiphiles to self-assemble into single-layered 2D nanosheets. Interestingly, the tuning of the $\pi-\pi$ stacking strength and the introduction of photoresponsive moieties into the mesogenic core of anionic bolaamphiphiles do not alter the formation of single-layered nanosheets. Subsequently, the terminal carboxylic moieties are converted into alkyl groups, thereby shielding the electrostatic repulsion and in turn yielding 2D multilayered nanosheets. Furthermore, by meticulously designing anionic bolaamphiphiles with the absence of either $\pi-\pi$ stacking or hydrogen-bonding interaction, irregular aggregates of anionic bolaamphiphiles are found to form. Taken together, these results clearly underpin the importance of electrostatic repulsions imparted by two negatively charged ends of anionic bolaamphiphiles in forming single-layered 2D nanosheets. Finally, intrinsically charged 2D nanosheets enable the deposition of oppositely charged metal nanoparticles *via* electrostatic interaction. This study not only provides a platform for creating single-layered and multilayered 2D organic nanosheets but also reveals the interrelation between the molecular structure of building blocks and their self-organized architectures.

RESULTS AND DISCUSSION

Molecular structure represents the most dominating factor in governing the self-assembly of molecules. In this context, a series of anionic bolaamphiphiles were designed and synthesized as depicted in Figure 1. In general, the molecular

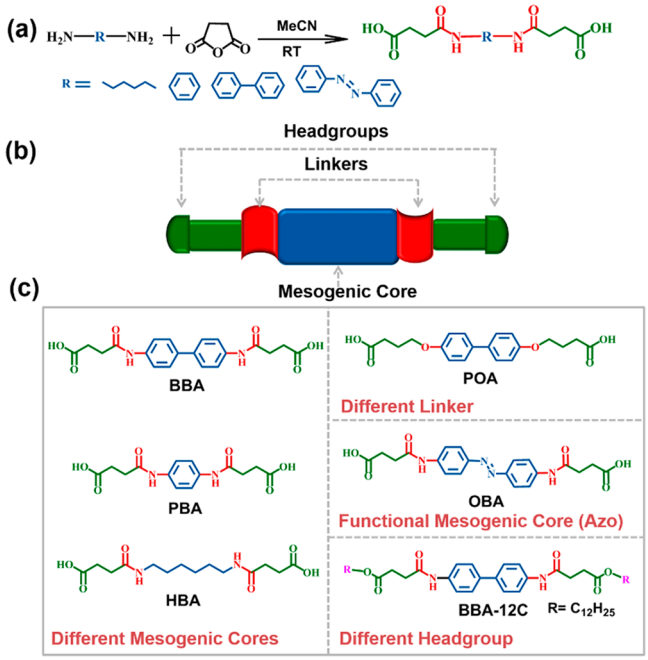

Figure 1. Investigation into the effect of the mesogenic core (blue), linker (red), and headgroup (green) on self-assembly of carboxylic acid-terminated bolaamphiphiles with various molecular structures. (a) One-step synthetic route of carboxylic acid-terminated bolaamphiphiles. (b) Schematic illustration of an anionic bolaamphiphile containing three complementary segments. (c) Diversified molecular structures of carboxylic acid-terminated bolaamphiphiles synthesized *via* four design principles, that is, varied mesogenic cores (left panel; from biphenyl in BBA, phenyl in PBA to hexyl in HBA), linkers (upper right panel; the ether linker), functional mesogenic core (central right panel; azobenzene in OBA), and headgroups (lower right panel; alkyl group: $-C_{12}H_{25}$).

structure of bolaamphiphiles comprises three segments: a rigid hydrophobic mesogenic core, two hydrophilic headgroups, and two linkers situated between the core moiety and headgroup (Figure 1b).

The primary bolaamphiphile, 4,4′-([1,1′-biphenyl]-4,4′-diylbis(azanediyl))bis(4-oxobutanoic acid) (denoted BBA), was synthesized *via* a one-step reaction with high yield (see Experimental Section and Schemes S1−S6 in the Supporting Information). It possesses a biphenyl group as the rigid core, two amide groups as the linkers, and two terminal carboxylic acid-containing headgroups. The self-assembly of BBA was performed in water containing an organic base, 1,1,3,3-tetramethylguanidine (TMG; a proven effective counterion for self-assembly of anionic bolaamphiphiles[28,29,36]). The presence of TMG transforms BBA into an anionic bolaamphiphile (*i.e.*, BBA^-) associated with a 1,1,3,3-tetramethylguanidinium (TMG^+) counterion due to the acid/base complexation reaction between BBA and TMG.

https://dx.doi.org/10.1021/acsnano.0c09693
ACS Nano 2021, 15, 3152−3160

Interestingly, the typical Tyndall effect was observed from the BBA^-/TMG^+ complex (referred to as BBA^-/TMG^+) solution. Subsequently, the reaction product was examined by transmission electronic microscopy (TEM) and atomic force microscopy (AFM). Figure 2a shows the representative 2D

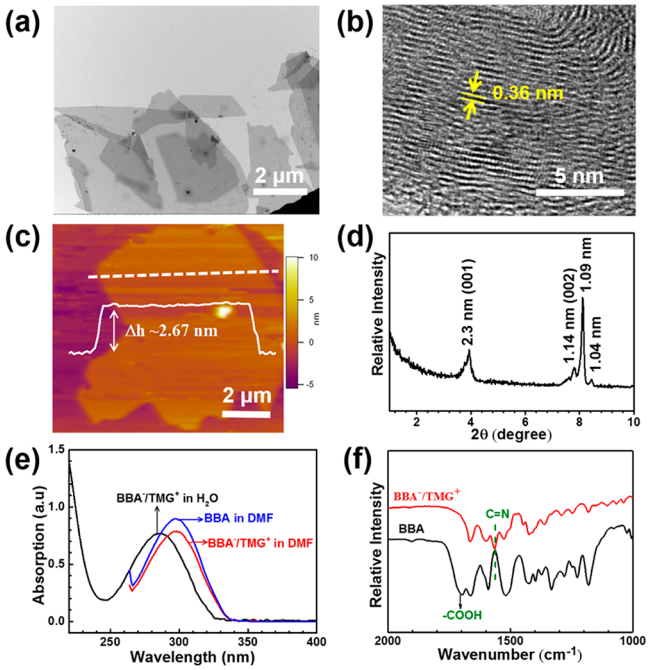

Figure 2. Characterization of a single-layered 2D organic nanosheet formed *via* self-assembly of BBA^-/TMG^+. (a) TEM and (b) HRTEM images of a single-layered 2D nanosheet composed of self-assembly of BBA^-/TMG^+ complexes. (c) AFM image and the corresponding cross-sectional analysis, (d) SAXRD pattern, (e) UV−vis absorption spectra, and (f) FT-IR spectra of a 2D single-layered BBA^-/TMG^+ nanosheet.

nanosheets formed in water with the lateral size ranging from a few to several tens of micrometers. The high-resolution TEM (HRTEM) measurement reveals that the nanosheet is highly crystalline with a lattice spacing of 0.36 nm (Figure 2b), which can be attributed to the $\pi-\pi$ stacking of the aromatic cores (upper left panel; Figure 1b). The nanosheet has an average thickness of 2.67 nm, as measured by AFM (Figure 2c), which is comparable to the extended length (2.2 nm) of the BBA molecule estimated by Chem 3D (Figure S1). This result suggests that a single-layered 2D organic nanosheet could be crafted in aqueous solution with a bolaamphiphile in the presence of TMG. It is noteworthy that the electrostatic repulsion of the ionic headgroups on the surface of the nanosheet plays a pivotal role in forming single-layered nanosheets.[28,29,36−39] The difference in the nanosheet thickness estimated by Chem 3D and measured by AFM may be ascribed to the presence of the TMG^+ counterions and water layer.[28,29] In order to further evaluate 2D organic nanosheets, a small-angle X-ray diffraction (SAXRD) study was conducted.[35,36] Figure 2d shows a dominant peak at $2\theta = 3.9°$, corresponding to a *d*-spacing of 2.3 nm, signifying the formation of a layered structure in the BBA^-/TMG^+ complex.[40,41] Notably, these single-layered 2D nanosheets created *via* the bottom-up self-assembly process can be stably dispersed in aqueous solution for months.

The formation of a single-layered 2D organic nanosheet composed of BBA^-/TMG^+ complexes may be rationalized as follows. The $\pi-\pi$ stacking of mesogenic biphenyl cores, intermolecular hydrogen-bonding between amide groups, hydrophobic interaction of the mesogenic core (*i.e.*, biphenyl) and linkers (*i.e.*, amides) of nearby BBAs, and electrostatic repulsion of anionic headgroups introduced due to the conversion of carboxyl end groups of BBA into charged BBA^-/TMG^+—all between neighboring BBAs—collectively self-assemble BBA^-/TMG^+ complexes into 2D supramolecular nanosheets. It is important to note that the judicious incorporation of electrostatic repulsions from BBA^-/TMG^+ on the surfaces of the single-layered 2D nanosheet greatly suppress their stacking into multilayered nanosheets,[28,29,36−39] thereby dispensing with the need for extra tedious exfoliation steps to yield single-layered nanosheets as in copious past works.[13,24,25]

To verify that the formation of 2D nanosheets is rendered by the synergistic noncovalent interactions discussed above, the nanosheets were also examined by UV−vis and Fourier-transform infrared (FT-IR) spectroscopies. The absorption of biphenyl groups of the BBA^-/TMG^+ assemblies appears at 298 nm in DMF and shifts to 285 nm when they are dispersed in water (Figure 2e). Such blue-shifted absorption signifies a more closely *H*-type stacking in a face-to-face mode during the formation of the 2D nanosheet due to the interaction of bolaamphiphiles, substantiating the emergence of $\pi-\pi$ stacking interactions of biphenyl cores during the self-assembly of BBA^-/TMG^+ in water,[40,42] which is in good agreement with the HRTEM result (Figure 2b). The complexation of BBA with TMG was revealed by the FT-IR measurement (Figure 2f). The peak at 1698 cm^{-1} can be assigned to the C═O absorption of carboxylic acid groups in pure BBA. Yet, for a 2D single-layered nanosheet composed of self-assembled BBA^-/TMG^+, the stretching vibration of C═O groups disappears, and a new peak at 1565 cm^{-1} emergeds, corresponding to the stretching vibration of C═N in TMG. Moreover, the stretching vibration of the C═O bond (amide I) and the N−H bending vibration of BBA^-/TMG^+ appear at lower wavenumbers of 1660 and 3333 cm^{-1}, respectively, suggesting the formation of hydrogen bonds between anionic bolaamphiphiles.[43−45] Furthermore, ^1H NMR spectra of BBA^-/TMG^+ also demonstrate the characteristic peaks of BBA and TMG (Figure S2).

In order to scrutinize the influence of the molecular structure of bolaamphiphiles on their self-assembly in aqueous solution, a collection of bolaamphiphiles other than BBA were rationally designed and synthesized (Figure 1c). First, instead of a biphenylene group in BBA, which possesses the stronger $\pi-\pi$ stacking interaction, another two bolaamphiphiles, that is, 4,4′-(1,4-phenylenebis(azanediyl))bis(4-oxobutanoic acid) (PBA) and 4,4′-(hexane-1,6-diylbis(azanediyl))bis(4-oxobutanoic acid) (HBA), were synthesized (see Experimental Section). They contain a phenylene group (single phenylene with weaker $\pi-\pi$ stacking interaction than that BBA; central left panel, Figure 1c) and a hexylene group (a flexible alkyl spacer without $\pi-\pi$ stacking interaction; lower left panel, Figure 1c), respectively, as the mesogenic core moiety. To ensure a consistent comparison, TMG was used as the base to form a TMG^+ counterion for all the bolaamphiphiles involved in this work. Similar to the case of BBA, the use of TMG converts PBA into an anionic bolaamphiphile (*i.e.*, PBA^-; see the Experimental Section). It is not surprising that the resulting

https://dx.doi.org/10.1021/acsnano.0c09693
ACS Nano 2021, 15, 3152−3160

PBA^-/TMG^+ complex could self-assemble into a 2D supramolecular nanosheet with a size of several microns (Figure 3a).

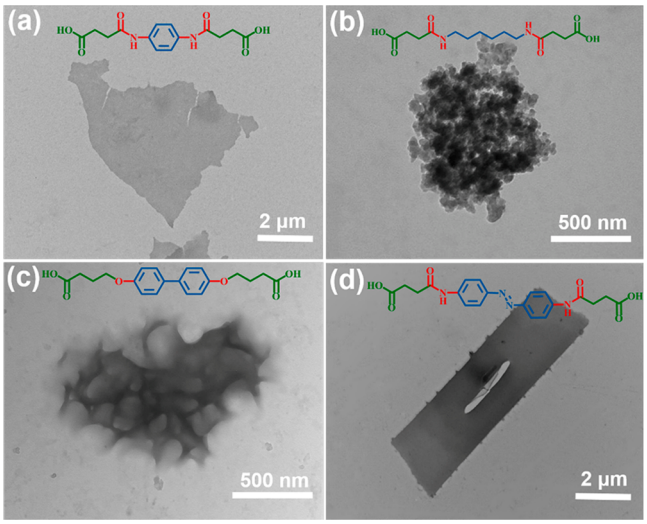

Figure 3. Effect of molecular structure of the mesogenic core on the self-assembly of bolaamphiphiles$^-$/TMG$^+$ complexes. TEM images of (a) a single-layered 2D nanosheet composed of self-assembled PBA$^-$/TMG$^+$ complexes, (b) aggregates of HBA$^-$/TMG$^+$ complexes, (c) aggregates of POA$^-$/TMG$^+$ complexes, and (d) a single-layered 2D nanosheet composed of self-assembled OBA$^-$/TMG$^+$ complexes. The corresponding molecular structures of PBA, HBA, POA, and OBA are shown as insets.

Although weaker than that of the biphenyl core as in BBA^-/TMG^+ (Figure 2a), the $\pi-\pi$ stacking interaction of the single phenylene core, in conjunction with the hydrogen-bonding, hydrophobic, and electrostatic repulsion interactions, drives the self-assembly of PBA^-/TMG^+ complexes into a single-layered 2D nanosheet in aqueous solution. In stark contrast, the HBA^-/TMG^+ complex formed by the acid/base complexation reaction between HBA and TMG yields particulate-like aggregates (Figure 3b). Taken together, these results clearly signify that the inclusion of a rigid mesogenic core and the associated $\pi-\pi$ stacking interactions between bolaamphiphiles$^-$/TMG$^+$ are of key importance in forming 2D supramolecular aggregates.

Subsequently, the influence of the linkers on self-assembly of bolaamphiphiles was also investigated. By rationally replacing the amide linkers with the ether groups, 4,4′-([1,1′-biphenyl]-4,4′-diylbis(oxy))dibutyric acid (denoted POA) was synthesized (upper right panel, Figure 1c; see the Experimental Section). Interestingly, despite both BBA and POA bolaamphiphiles containing rigid hydrophobic biphenyl groups, their self-assembly behaviors are distinctly different in aqueous solution. The BBA^-/TMG^+ complexes self-assemble into single-layered 2D nanosheets (Figure 2a), yet POA^-/TMG^+ complexes, formed from the acid/base complexation reaction of POA and TMG, result in ill-defined aggregates (Figure 3c). Clearly, the substitution of the amide linkers by ether linkers eliminates the hydrogen-bonding interactions between POA^-/TMG^+ complexes, thereby leading to the formation of aggregates. Nonetheless, the results discussed above (Figure 3b,c and Figures S3−S8) reveal the importance of $\pi-\pi$ stacking and hydrogen bonding as well as their synergy in creating 2D supramolecular nanosheets *via* self-assembly of bolaamphiphiles$^-$/TMG$^+$ in aqueous solution. The FT-IR and UV−vis spectroscopies were also used to evaluate the intermolecular hydrogen-bonding and $\pi-\pi$ stacking interactions of the self-assembled complexes (Figures S9−S16), and the results are summarized in Tables S1 and S2, respectively. The sizes of the resulting self-assembled complexes (Figures S17−S21) were characterized by dynamic light scattering (DLS) and are comparable with the TEM results.

We note that in order to introduce more functionalities into the bolaamphiphile, the biphenyl group of BBA was substituted with the azobenzene group, yielding photoresponsive anionic bolaamphiphile (*E*)-4,4′-((diazene-1,2-diylbis(4,1-phenylene))bis(azanediyl))bis(4-oxobutanoic acid) (denoted OBA; see the Experimental Section). It is well-known that the trans-isomer of azobenzene has a planar rigid configuration, making it an ideal building block to construct 2D structures.[42,46,47] The implementation of the OBA^-/TMG^+ complex as the building block synthesized by the reaction of BOA and TMG produces several-micron-sized, single-layered 2D nanosheets consisting of OBA^-/TMG^+ complexes (Figure 3d). This result suggests that changing the biphenyl core to azobenzene has negligible influence on the self-assembly morphology due to the comparable $\pi-\pi$ stacking interaction strength of azobenzene moieties to that of the biphenyl moieties. The photoisomerization of the azobenzene moieties in 2D OBA^-/TMG^+ nanosheets was monitored by UV−vis spectroscopy. The trans-to-cis isomerization of the azobenzene moieties is highly reversible upon alternating irradiation with UV and visible light (Figures S22 and S23). However, the morphology of the 2D OBA^-/TMG^+ nanosheets cannot be reversibly transformed during the photoisomerization. After UV irradiation of the 2D nanosheet solution, it translates into an irregular structure, which was found to remain under visible light irradiation (Figure S24). This can be ascribed to the breaking of intermolecular hydrogen bonding during photoisomerization from *trans*- to *cis*-azobenzene under UV irradiation in conjunction with a *nonplanar cis*-azobenzene conformation. The visible light cannot induce the restoration of the 2D nanosheet morphology; this may be because the intermolecular hydrogen bonding in UV-irradiated aggregates could not be broken and reconstructed into a regular morphology under visible light irradiation.

As discussed above, ionic headgroups at both ends of bolaamphiphiles are crucial for yielding single-layered 2D nanosheets. In order to elucidate the effect of ionic headgroups, didodecyl 4,4′-([1,1′-biphenyl]-4,4′-diylbis-(azanediyl))bis(4-oxobutanoate) (denoted BBA-12C; see the Experimental Section) was synthesized *via* the esterification reaction between BBA and $CH_3(CH_2)_{10}CH_2Br$ using TMG as a promoter at room temperature.[48−50] Compared to amphiphilic BBA, BBA-12C is hydrophobic and the ionic headgroups are shielded with alkyl groups, which screen the electrostatic repulsion. Figure 4a shows the TEM image of several-micron-sized multilayered nanosheets formed, where the layers are indicated with the respective white arrows. The thickness of the nanosheets was measured to be approximately 35.8 nm by AFM (Figures 4b,c), which is much larger than the extended length of BBA-12C (5.23 nm, estimated by Chem 3D and shown in Figure S25), revealing a multilayered structure of nanosheets.

The multilayered 2D nanosheets were also examined by SAXRD. A strong and sharp diffraction peak at $2\theta = 1.86°$ corresponds to a *d*-spacing of 4.75 nm (indexed to (001)) (Figure 4d). The *d*-spacing of the (001) plane slightly deviates

https://dx.doi.org/10.1021/acsnano.0c09693
ACS Nano 2021, 15, 3152−3160

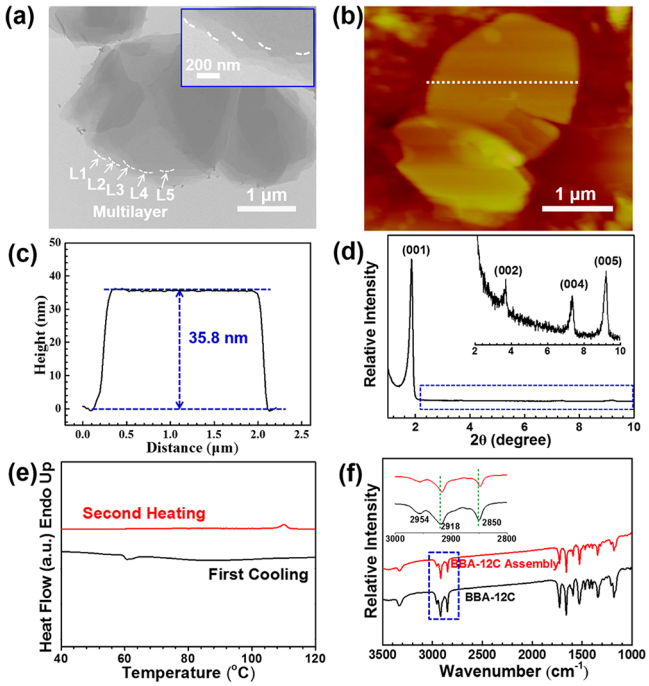

Figure 4. Morphological and structural study of multilayered 2D nanosheets formed by self-assembly of BBA-12C in the absence of electrostatic repulsion. (a) TEM image and high-magnification TEM image, (b) AFM image, (c) corresponding cross-sectional analysis taken along the white line in (b), (d) SAXRD pattern, (e) DSC profiles, and (f) FT-IR spectra of a multilayered 2D nanosheet composed of self-assembled BBA-12C.

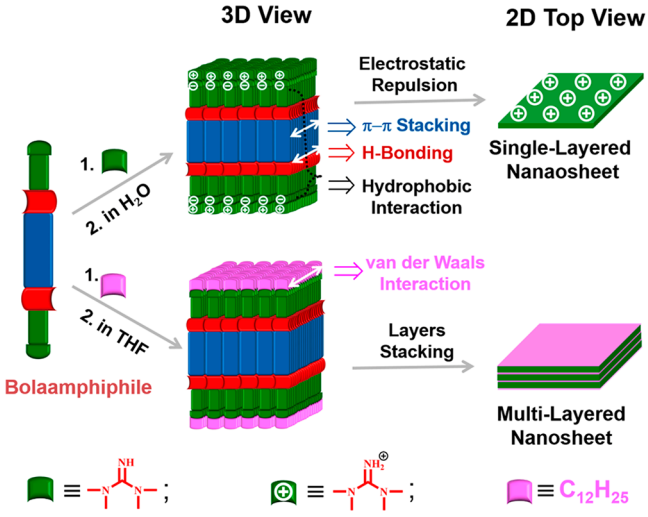

Figure 5. Possible mechanism for the formation of self-assembled single-layered and multilayered nanosheets from bolaamphiphiles due to the synergy of a suite of noncovalent interactions (*i.e.*, $\pi-\pi$ stacking, hydrophobic, hydrogen-bonding, and electrostatic repulsion interactions).

from the extended length of BBA-12C (5.23 nm), which can be attributed to the oblique arrangement of BBA-12C with a longer alkyl chain within the nanosheet.[36] It is notable that the diffraction pattern also shows periodic peaks at 3.86°, 7.34°, and 9.21° with the corresponding *d*-spacings of 2.38, 1.20, and 0.96 nm according to Bragg's equation. The ratio of the *d*-spacing is 1:1/2:1/4:1/5, suggesting a periodical lamellar structure of nanosheets.[46,47] Figure 4e shows the differential scanning calorimetry (DSC) result of multilayered 2D nanosheets, where a sharp endothermic peak can be seen at 110 °C during the heating cycle, indicative of phase transformation of the multilayered nanosheets from a highly ordered crystal with strong van der Waals interaction (lower left panel; Figure 5) to a disordered state in BBA-12C.[23,46] Clearly, these results manifest that the electrostatic repulsion dictates the creation of single-layered supramolecular nanosheets over multilayered counterparts.[28,29,36−38]

An FT-IR study on the multilayered nanosheets shows two peaks located at 1727 and 1657 cm^{-1} (Figure 4f), which can be assigned to the stretching vibration of C═O in the ester bond and the amide I mode, respectively. The low frequencies of amide I and N−H bending vibration (3329 cm^{-1}) modes suggest the formation of strong hydrogen bonding between molecules. It is well-known that CH_2 asymmetric and symmetric stretching vibrations can be used to depict the packing and conformation of alkyl chains. Prior to self-assembly, BBA-12C displays $\nu_{as}(CH_3)$, $\nu_{as}(CH_2)$, and $\nu_s(CH_2)$ at 2954, 2918, and 2850 cm^{-1}, respectively (Figure 4f). After self-assembly, the asymmetric and symmetric stretching vibrations of CH_2 appear at 2916 and 2848 cm^{-1}, respectively; the lowered frequencies suggest the all-trans conformation of hydrocarbon chains.[22,46] Taken together, these results suggest that BBA-12C molecules are closely and orderly packed within the 2D nanosheets in a multilayered manner.

Table S3 summarizes the noncovalent interactions of bolaamphiphiles and the as-formed morphologies after self-assembly. Clearly, single-layered 2D nanosheets can be crafted due to the collective interaction among the $\pi-\pi$ stacking, intermolecular hydrogen-bonding, hydrophobic, and electrostatic repulsion interactions. On the basis of a suite of microscopic, spectral, and XRD studies, the underlying mechanism governing the nanosheet formation may be conceived as follows. Rod-like bolaamphiphiles containing a rigid aromatic core and two amide groups tend to form 2D supramolecular nanosheets due to a series of favorable intermolecular interactions, including the $\pi-\pi$ stacking of phenyl or biphenyl groups, hydrogen bonding of amide groups, and hydrophobic interactions of the skeleton (*i.e.*, one mesogenic core and two linkers; Figure 1b) in an aqueous solution (Figure 5). The meticulous incorporation of anionic headgroups at the two hydrophilic ends of bolaamphiphiles renders the formation of single-layered 2D nanosheets as a result of strong electrostatic repulsions between adjacent nanosheets, thereby leading to stable single-layered nanosheets in an aqueous solution (upper panels; Figure 5). In the absence of ionic headgroups (*via* converting terminal carboxylic groups to hydrophobic alkyl groups), no electrostatic repulsion will be experienced among 2D nanosheets, thus resulting in the stacked multilayered structure to reduce the overall surface areas of nanosheets (lower panels; Figure 5).

It has been demonstrated that negatively charged Au nanoparticles (NPs) readily absorb on 2D polymer single crystals *via* the coordination interaction between the pendant pyridyl groups of the polymer and the terminal carboxylic acid-containing ligands on the Au NP surface.[51] To examine the surface functionality of 2D organic nanosheets, that is, associated with positive moieties (*i.e.*, quaternary amine in 1,1,3,3-tetramethylguanidinium (TMG^+)), the carboxylic acid-containing ligand-capped Au NPs (*i.e.*, negatively charged ligand) were employed to facilitate the anchoring of Au NPs

https://dx.doi.org/10.1021/acsnano.0c09693
ACS Nano 2021, 15, 3152−3160

on the surface of 2D nanosheets *via* electrostatic attraction (see Experimental Section). The Au NPs with an average size of 19 ± 0.8 nm (Figure S26a) exhibit a characteristic surface plasmon resonance (SPR) peak at 532 nm without aggregation in an aqueous solution (Figure S26d). When deposited on the surface of 2D BBA^-/TMG^+ nanosheets at a low amount, Au NPs can be seen to situate individually yet closely to each other on the surface of the 2D nanosheet *via* electrostatic interaction (BBA^-/TMG^+@Au-0.5 sample; see Experimental Section; Figure S26b), with which an additional absorption peak appears in the UV−vis spectrum due to the plasmonic coupling among adjacent Au NPs (Figure S26d). As the amount of Au NPs increases, more Au NPs are anchored on the surface of the 2D nanosheet (Figure S26c). A broad SPR peak in the long-wavelength region emerges due to the stronger plasmonic coupling of Au NPs decorated on the 2D nanosheet[52−54] (BBA^-/TMG^+@Au-1.0 sample; see the Experimental Section).

CONCLUSION

In summary, we synthesized an assortment of anionic bolaamphiphiles with varied molecular structures (*via* tailoring their mesogenic core, linker, and headgroup) and functionalities (*e.g.*, introducing photoresponsive moieties) as building blocks that experience different synergy of a set of intermolecular interactions, leading to disparate 2D self-assembled architectures. The scrutiny of the correlation between rationally designed anionic bolaamphiphiles and the resulting 2D self-assemblies reveals that the aromatic $\pi-\pi$ stacking, hydrophobic, and hydrogen-bonding interactions are crucial in forming 2D nanosheets. The bola-containing molecular structures of building blocks render exquisite control over the self-assembly process and 2D nanosheet formation. Moreover, investigation into the self-assembly behaviors of bolaamphiphiles unveils that the electrostatic repulsion plays a key role in creating single-layered 2D organic nanosheets. By contrast, the absence of electrostatic repulsion *via* converting two hydrophilic bola-ends into alkyl chains results in multilayered 2D nanosheets. Furthermore, single-layered 2D nanosheets can be functionalized with Au nanoparticles *via* electrostatic attraction. This study demonstrates the molecular engineering of bolaamphiphiles of the same type to form homogeneous 2D organic nanosheets. By extension, the implementation of bolaamphiphiles of two or more different types and their self-assembly may lead to heterogeneous 2D organic nanosheets with complex functionalities. They can be subsequently decorated with metal or metal oxide nanocrystals of interest to yield hybrid organic/inorganic 2D nanomaterials for catalysis, molecular imaging and sensing, and energy storage, among other areas.

EXPERIMENTAL SECTION

Materials. Most of the chemical reagents were purchased from Sinopharm Chemical Reagent Co., Ltd., and utilized as received unless indicated otherwise. 1,1,3,3-Tetramethylguanidine was purchased from TCI Chemicals and distilled under reduced pressure. The *p*-aminoacetanilide, 4,4′-dihydroxybiphenyl, and ethyl 4-bromobutyrate were obtained from Aladdin Chemical Reagent Co., Ltd. All other chemicals were analytical-grade reagents and used directly without further purification.

Synthesis of 4,4′-([1,1′-Biphenyl]-4,4′-diylbis(azanediyl))bis(4-oxobutanoic acid). In a 250 mL round-bottom flask, a solution of benzidine (1.842 g, 10 mmol) in MeCN (100 mL) was added at room temperature, followed by the dropwise addition of succinic anhydride (2.40 g, 24 mmol); precipitates were formed immediately. After stirring for 24 h, gray solids were filtered and washed with MeCN (3.805 g, 99%). The compound was used without further purification and denoted BBA (Scheme S1). The physical data for BBA (Figures S27 and S28): ^{1}H NMR (300 MHz, *d*-DMSO): δ (ppm) 12.13 (s, 2H, **COOH**), 10.03 (s, 2H, CO**NH**), 7.64 (d, J = 7.7 Hz, 4H, Ar), 7.59 (d, J = 7.6 Hz, 4H, Ar), 2.56 (d, J = 4.3 Hz, 4H, $-\mathbf{CH_2}-\mathbf{CH_2}-$); ^{13}C NMR (300 MHz, *d*-DMSO) δ (ppm) 173.9, 170.2, 138.4, 134.2, 126.4, 119.3, 31.1, 28.9; HRMS (ESI) m/z calcd for $C_{20}H_{20}N_2O_6$ [M + H$^+$] 385.1394, found 385.1394.

Synthesis of 4,4′-(1,4-Phenylenebis(azanediyl))bis(4-oxobutanoic acid). PBA (Scheme S2) was synthesized in a similar procedure to BBA, with *p*-phenylenediamine as raw material (Figures S29 and S30). ^{1}H NMR (300 MHz, *d*-DMSO) δ (ppm) 12.05 (s, 2H, **COOH**), 9.87 (s, 2H, CO**NH**), 7.48 (s, 4H, Ar), 2.56 (d, J = 4.3 Hz, 4H, $-\mathbf{CH_2}-\mathbf{CH_2}-$); ^{13}C NMR (300 MHz, *d*-DMSO) δ (ppm) 173.9, 168.9, 132.2, 119.1, 30.9, 28.6; HRMS (ESI) m/z calcd for $C_{14}H_{16}N_2O_6$ [M + H$^+$] 309.1081, found 309.1081.

Synthesis of 4,4′-(Hexane-1,6-diylbis(azanediyl))bis(4-oxobutanoic acid). HBA (Scheme S3) was synthesized in a similar procedure to BBA, with hexamethylenediamine as raw material (Figures S31 and S32). ^{1}H NMR (300 MHz, *d*-DMSO) δ (ppm) 9.87 (s, 2H, CONH), 3.00 (dd, J = 12.4, 6.4 Hz, 4H, $-$CONH**CH$_2$**$-$), 2.40 (t, J = 6.6 Hz, 4H, $-\mathbf{CH_2}CH_2CONH-$), 2.28 (t, J = 6.7 Hz, 4H, $-CH_2\mathbf{CH_2}CONH-$), 1.34 (t, J = 5.7 Hz, 4H, $-CH_2\mathbf{CH_2}CH_2NH-$), 1.23 (s, 4H, $-\mathbf{CH_2}CH_2CH_2NH-$); ^{13}C NMR (300 MHz, *d*-DMSO) δ (ppm) 173.9, 170.7, 38.5, 30.1, 29.2, 28.9, 26.0. HRMS (ESI) m/z calcd for $C_{14}H_{24}N_2O_6$ [M + H$^+$] 317.1707, found 317.1713.

Synthesis of (*E*)-4,4′-((Diazene-1,2-diylbis(4,1-phenylene))bis(azanediyl))bis(4-oxobutanoic acid). In a round-bottomed tube, a solution of 4,4′-diaminoazobenzene (1 g, 4.71 mmol) in MeCN (100 mL) was added at room temperature, followed by the dropwise addition of succinic anhydride (1.895 g, 18.84 mmol); yellow precipitates were formed immediately. After stirring for 24 h, yellow solids were filtered and washed with MeCN. The compound was used without further purification. The as-obtained compound is denoted OBA (Scheme 4; Figures S33 and S34). Yield: 97%. ^{1}H NMR (300 MHz, *d*-DMSO) δ (ppm) 12.96 (s, 2H, COOH), 10.68 (s, 2H, CONH), 7.86 (d, J = 7.7 Hz, 4H, Ar), 7.85 (d, J = 7.6 Hz, 4H, Ar), 6.49 (d, J = 6.5 Hz, 2H, double bond), 6.33 (d, J = 6.3 Hz, 2H, double bond); ^{13}C NMR (300 MHz, *d*-DMSO) δ 168.7, 147.5, 142.0, 123.4, 119.1, 24.2; HRMS (ESI) m/z calcd for $C_{20}H_{20}N_4O_6$ [M + H$^+$] 413.1456, found 413.1461.

Synthesis of Diethyl 4,4′-([1,1′-Biphenyl]-4,4′-diylbis(oxy))dibutyrate (Denoted Intermediate 1 in Scheme 5). In a three-necked flask, KOH powder (0.561 g, 10 mmol) was dispersed in DMF (50 mL) under vigorous stirring. After fully deoxygenated with nitrogen, 4,4′-dihydroxybiphenyl (0.372 g, 2 mmol) was added quickly. Then, ethyl 4-bromobutyrate (1.2 mL, 8 mmol) was slowly injected into the solution. The resulting mixture was stirred overnight at 70 °C. After cooling in an ice−water bath, the reaction mixture was poured into cold water, and a precipitate was formed. The final product was filtered and washed with water and hexane, respectively. White powder was collected after vacuum-drying (denoted Intermediate 1; Figures S35 and S36). Yield: 85.6%. ^{1}H NMR (300 MHz, $CDCl_3$) δ (ppm) 7.45 (d, J = 8.6 Hz, 4H, Ar), 6.93 (d, J = 8.6 Hz, 4H, Ar), 4.15 (q, J = 7.1 Hz, 4H, $-CH_2CH_2\mathbf{CH_2}-$), 4.04 (t, J = 5.9 Hz, 4H, $CH_3\mathbf{CH_2}-$), 2.53 (t, J = 7.2 Hz, 4H, $-\mathbf{CH_2}CH_2CH_2-$), 2.12 (t, J = 6.6 Hz, 4H, $-CH_2\mathbf{CH_2}CH_2-$), 1.26 (t, J = 7.1 Hz, 6H, $\mathbf{CH_3}CH_2-$); ^{13}C NMR (300 MHz, $CDCl_3$) δ (ppm) 173.39, 158.1, 133.7, 127.9, 114.9, 66.9, 60.6, 31.0, 24.8, 14.4; HRMS (ESI) m/z calcd for $C_{24}H_{30}O_6$ [M + H$^+$] 415.2042, found 415.2057.

Synthesis of 4,4′-([1,1′-Biphenyl]-4,4′-diylbis(oxy))dibutyric Acid. The product Intermediate 1 (0.415 g, 1 mmol) was dissolved in a mixture of THF (50 mL) and CH_3OH (50 mL), and then NaOH (0.2 g, 5 mmol) was added to the mixture and refluxed for 24 h. After cooling in an ice−water bath, the reaction mixture was acidified with HCl solution. Thereafter, the solution was poured into cold water and a precipitate was formed. The final product was filtered and washed with water until the filtrate was neutral. White powder was collected

https://dx.doi.org/10.1021/acsnano.0c09693
ACS Nano 2021, 15, 3152−3160

after vacuum-drying. Yield: 98.1%. The as-obtained compound is denoted POA (Scheme 5; Figures S37 and S38). ^{1}H NMR (300 MHz, *d*-DMSO) δ (ppm) 12.3 (s, 2H, COOH), 7.63 (d, J = 7.2 Hz, 4H, Ar), 7.08 (d, J = 7.3 Hz, 4H, Ar), 4.11 (s, 1H, $-CH_2CH_2\mathbf{CH_2}-$), 2.61 (s, 4H, $-\mathbf{CH_2}CH_2CH_2-$), 2.20−1.89 (m, 4H, $-CH_2\mathbf{CH_2}CH_2-$); ^{13}C NMR (300 MHz, *d*-DMSO) δ (ppm) 174.1, 157.6, 132.3, 127.2, 114.8, 85.5, 66.6, 30.2, 24.3; HRMS (ESI) m/z calcd for $C_{20}H_{22}O_6$ [M + H$^+$] 359.1489, found 359.1487.

Synthesis of Didodecyl 4,4′-([1,1′-Biphenyl]-4,4′-diylbis(azanediyl))bis(4-oxobutanoate). In a 100 mL round-bottomed flask, 4,4′-([1,1′-biphenyl]-4,4′-diylbis(azanediyl))bis(4-oxobutanoic acid) (0.769 g, 2 mmol) was dissolved in DMF (20 mL); then 1,1,3,3-tetramethylguanidine (507 μL, 4 mmol) was added to the solution and stirred for 10 min. Then 1-bromododecane (1.5 mL, 6 mmol) in THF (10 mL) was added to the mixture and stirred at room temperature for 24 h. Thereafter, the reaction mixture was poured into cold water and a precipitate was formed. The final product was filtered and washed with water and diethyl ether, respectively. Gray solids were obtained after vacuum-drying. Yield: 88.2%. The as-obtained compound is denoted BBA-12C (Scheme S6; Figure S39). The concentration in $CDCl_3$ is very low at room temperature, thus making ^{13}C characterization impossible. ^{1}H NMR (300 MHz, $CDCl_3$) δ (ppm) 7.52 (dd, J = 20.0, 8.0 Hz, 8H, Ar), 4.10 (t, J = 6.5 Hz, 4H, $-\mathbf{CH_2}OOC-$), 2.76 (d, J = 5.4 Hz, 4H, $-OCCH_2\mathbf{CH_2}CO-$), 2.69 (d, J = 5.1 Hz, 4H, $-OC\mathbf{CH_2}CH_2CO-$), 1.61 (d, J = 6.4 Hz, 4H, $-\mathbf{CH_2}CH_2OOC-$), 1.25 (s, 36H, $(-\mathbf{CH_2}-)_9$), 0.93 (t, J = 6.6 Hz, 6H, $\mathbf{CH_3}-$); HRMS (ESI) m/z calcd for $C_{44}H_{68}N_2O_6$ [M + H$^+$] 721.5150, found 721.5156.

Formation of Single-Layered 2D Supramolecular Nanosheets *via* Self-Assembly of Bolaamphiphiles. In a typical procedure, bolaamphiphiles (20 mg) were dispersed in 10 mL of water and sonicated 30 min; then 2 equiv of TMG was added to the dispersion and sonicated for another 5 min. The solution turned transparent immediately. The aqueous solution was allowed to stand for 24 h without stirring at room temperature. Finally, the solution was transferred to a dialysis tube (molecular weight cutoff: 7000 g/mol) and dialyzed against deionized water for 48 h. For the bolaamphiphiles BBA, PBA, HBA, POA, and OBA, the as-obtained complexes with TMG are denoted BBA$^-$/TMG$^+$, PBA$^-$/TMG$^+$, HBA$^-$/TMG$^+$, POA$^-$/TMG$^+$, and OBA$^-$/TMG$^+$, respectively.

Preparation of Multilayered 2D Supramolecular Nanosheets *via* Self-Assembly of BBA-12C. A suspension of BBA-12C in THF (concentration: 1 mg/mL) was heated to reflux until all the solids were completely dissolved to form a colorless, clear solution. The solution was then allowed to cool gradually to room temperature to yield multilayered 2D supramolecular nanosheets.

Synthesis of Au Nanoparticles. A 10 mg amount of $HAuCl_4$ was dissolved in 100 mL of deionized water. The solution was then heated with vigorous stirring under reflux. A 10 mL portion of a sodium citrate solution (10 mg/mL) was then added. The mixture was stirred under reflux for 1 h. Finally, the resulting colloid solution was slowly cooled to room temperature. The solution was dialyzed against DI water with a dialysis tube (molecular weight cutoff, 7000 g/mol) for 2 days. The final volume was concentrated to 50 mL.

Decoration of 2D Nanosheets with Au NPs. A 5 mL amount of the freshly prepared Au NP solution was slowly added into 10 mL of the 2D BBA$^-$/TMG$^+$ nanosheet solution at room temperature. The mixture was incubated at room temperature for 24 h without stirring to form BBA$^-$/TMG$^+$@Au-0.5. When 10 mL of the freshly prepared Au NP solution was added to 10 mL of the BBA$^-$/TMG$^+$ nanosheet solution, the nanocomposite BBA$^-$/TMG$^+$@Au-1 was obtained.

Characterization. All NMR spectra were recorded on a Bruker AVANCEII spectrometer (resonance frequency of 300 MHz for ^{1}H and ^{13}C) operated in the Fourier transform mode with TMS as internal standard. Multiplets are denoted as s (singlet), bs (broad singlet), d (duplet), t (triplet), and m (multiplet), and given values are positioned in the center of a peak. FT-IR spectra were obtained in the spectral range from 4000 to 400 cm^{-1} with a Thermo Nicolet 6700. UV−vis spectra of solutions were measured with a Shimadzu UV 3600 UV−Nir−NIR spectrometer at room temperature. High-resolution mass spectra (HRMS) were recorded on a Thermo Q Exactive HF mass spectrometer in positive mode. XRD patterns were recorded by using a Philips X'Pert Pro Super diffractometer with Cu Kα radiation (λ = 1.541 78 Å). DSC measurements were carried out at a heating rate of 10 °C/min under nitrogen with a TA Q2000, TA Instruments. AFM images were taken with a Veeco DI Innova in tapping mode on coated SiO_2/Si-wafer pieces. The morphologies of the 2D polymers were characterized by TEM using a JEOL-2010 transmission electron microscope operated at 200 kV. The samples were prepared by placing a droplet of solution onto a carbon-coated copper grid, followed by air-drying. The size distributions of bolaamphiphiles in aqueous solution were characterized by DLS (Wyatt DyanoPro NanoStar Dynamic Light Scattering) at 25 °C.

ASSOCIATED CONTENT

Supporting Information

The Supporting Information is available free of charge at https://pubs.acs.org/doi/10.1021/acsnano.0c09693.

Additional information on synthesis of bolaamphiphiles and their assemblies, TEM images, FT-IR, UV−vis, DLS, and NMR spectra, as well as the summarized tables about structure and morphologies (PDF)

AUTHOR INFORMATION

Corresponding Author

Zhiqun Lin − *School of Materials Science and Engineering, Georgia Institute of Technology, Atlanta, Georgia 30332, United States;* orcid.org/0000-0003-3158-9340; Email: Zhiqun.lin@mse.gatech.edu

Author

Zili Li − *School of Materials Science and Engineering, Georgia Institute of Technology, Atlanta, Georgia 30332, United States*

Complete contact information is available at: https://pubs.acs.org/10.1021/acsnano.0c09693

Notes

The authors declare no competing financial interest.

ACKNOWLEDGMENTS

This work is supported by the NSF (Chemistry 1903957).

REFERENCES

(1) Lin, Y.; Thomas, M. R.; Gelmi, A.; Leonardo, V.; Pashuck, E. T.; Maynard, S. A.; Wang, Y.; Stevens, M. M. Self-Assembled 2D Free-Standing Janus Nanosheets with Single-Layer Thickness. *J. Am. Chem. Soc.* **2017**, *139*, 13592−13595.

(2) Zhang, X.; Gong, C.; Akakuru, O. U.; Su, Z.; Wu, A.; Wei, G. The Design and Biomedical Applications of Self-Assembled Two-Dimensional Organic Biomaterials. *Chem. Soc. Rev.* **2019**, *48*, 5564−5595.

(3) Krieg, E.; Bastings, M. M.; Besenius, P.; Rybtchinski, B. Supramolecular Polymers in Aqueous Media. *Chem. Rev.* **2016**, *116*, 2414−2477.

(4) Han, L.; Wang, M.; Jia, X.; Chen, W.; Qian, H.; He, F. Uniform Two-Dimensional Square Assemblies from Conjugated Block Copolymers Driven by π-π Interactions with Controllable Sizes. *Nat. Commun.* **2018**, *9*, 865.

(5) Feng, X.; Shen, B.; Sun, B.; Kim, J.; Liu, X.; Lee, M. Single-Layered Chiral Nanosheets with Dual Chiral Void Spaces for Highly Efficient Enantiomer Absorption. *Angew. Chem., Int. Ed.* **2020**, *59*, 11355−11359.

(6) Boott, C. E.; Nazemi, A.; Manners, I. Synthetic Covalent and Non-Covalent 2D Materials. *Angew. Chem., Int. Ed.* **2015**, *54*, 13876−13894.
(7) Hu, B.; Sun, S.; Wu, B.; Wu, P. Colloidally Stable Monolayer Nanosheets with Colorimetric Responses. *Small* **2019**, *15*, 1804975.
(8) Wang, L.; Zhang, Y.; Chen, L.; Xu, H.; Xiong, Y. 2D Polymers as Emerging Materials for Photocatalytic Overall Water Splitting. *Adv. Mater.* **2018**, *30*, 1801955.
(9) Bai, W.; Jiang, Z.; Ribbe, A. E.; Thayumanavan, S. Smart Organic Two-Dimensional Materials Based on a Rational Combination of Non-Covalent Interactions. *Angew. Chem.* **2016**, *128*, 10865−10869.
(10) Liang, Y.; Zhu, Y.; Liu, C.; Lee, K.-R.; Hung, W.-S.; Wang, Z.; Li, Y.; Elimelech, M.; Jin, J.; Lin, S. Polyamide Nanofiltration Membrane with Highly Uniform Sub-Nanometre Pores for Sub-1 Å Precision Separation. *Nat. Commun.* **2020**, *11*, 2015.
(11) Ariga, K.; Lee, M. V.; Mori, T.; Yu, X.-Y.; Hill, J. P. Two-Dimensional Nanoarchitectonics Based on Self-Assembly. *Adv. Colloid Interface Sci.* **2010**, *154*, 20−29.
(12) Govindaraju, T.; Avinash, M. Two-Dimensional Nanoarchitectonics: Organic and Hybrid Materials. *Nanoscale* **2012**, *4*, 6102−6117.
(13) Lange, R. Z.; Synnatschke, K.; Qi, H.; Huber, N.; Hofer, G.; Liang, B.; Huck, C.; Pucci, A.; Kaiser, U.; Backes, C. Enriching and Quantifying Porous Single Layer 2D Polymers by Exfoliation of Chemically Modified Van Der Waals Crystals. *Angew. Chem., Int. Ed.* **2020**, *59*, 5683−5695.
(14) Song, D.-P.; Li, C.; Colella, N. S.; Xie, W.; Li, S.; Lu, X.; Gido, S.; Lee, J.-H.; Watkins, J. J. Large-Volume Self-Organization of Polymer/Nanoparticle Hybrids with Millimeter-Scale Grain Sizes Using Brush Block Copolymers. *J. Am. Chem. Soc.* **2015**, *137*, 12510−12513.
(15) Jin, H.; Jiao, F.; Daily, M. D.; Chen, Y.; Yan, F.; Ding, Y.-H.; Zhang, X.; Robertson, E. J.; Baer, M. D.; Chen, C.-L. Highly Stable and Self-Repairing Membrane-Mimetic 2D Nanomaterials Assembled from Lipid-Like Peptoids. *Nat. Commun.* **2016**, *7*, 12252.
(16) Qiu, H.; Gao, Y.; Boott, C. E.; Gould, O. E.; Harniman, R. L.; Miles, M. J.; Webb, S. E.; Winnik, M. A.; Manners, I. Uniform Patchy and Hollow Rectangular Platelet Micelles from Crystallizable Polymer Blends. *Science* **2016**, *352*, 697−701.
(17) Wei, Y.; Tian, J.; Zhang, Z.; Zhu, C.; Sun, J.; Li, Z. Supramolecular Nanosheets Assembled from Poly(ethylene glycol)-*b*-Poly(N-(2-phenylethyl) glycine) Diblock Copolymer Containing Crystallizable Hydrophobic Polypeptoid: Crystallization Driven Assembly Transition from Filaments to Nanosheets. *Macromolecules* **2019**, *52*, 1546−1556.
(18) Wang, S.-P.; Lin, W.; Wang, X.; Cen, T.-Y.; Xie, H.; Huang, J.; Zhu, B.-Y.; Zhang, Z.; Song, A.; Hao, J. Controllable Hierarchical Self-Assembly of Porphyrin-Derived Supra-Amphiphiles. *Nat. Commun.* **2019**, *10*, 1399.
(19) Ghosh, S.; Philips, D. S.; Saeki, A.; Ajayaghosh, A. Nanosheets of an Organic Molecular Assembly from Aqueous Medium Exhibit High Solid-State Emission and Anisotropic Charge-Carrier Mobility. *Adv. Mater.* **2017**, *29*, 1605408.
(20) Huang, J.; Wang, S.; Wu, G.; Yan, L.; Dong, L.; Lai, X.; Yin, S.; Song, B. Mono-Molecule-Layer Nano-Ribbons Formed by Self-Assembly of Bolaamphiphiles. *Soft Matter* **2014**, *10*, 1018−1023.
(21) Yin, S.; Dong, L.; Xia, Y.; Dong, B.; He, X.; Chen, D.; Qiu, H.; Song, B. Controlled Self-Assembly of a Pyrene-Based Bolaamphiphile by Acetate Ions: From Nanodisks to Nanofibers by Fluorescence Enhancement. *Soft Matter* **2015**, *11*, 4424−4429.
(22) Wu, G.; Verwilst, P.; Liu, K.; Smet, M.; Faul, C. F.; Zhang, X. Controlling the Self-Assembly of Cationic Bolaamphiphiles: Counter-ion-Directed Transitions from 0D/1D to Exclusively 2D Planar Structures. *Chem. Sci.* **2013**, *4*, 4486−4493.
(23) Wu, G.; Thomas, J.; Smet, M.; Wang, Z.; Zhang, X. Controlling the Self-Assembly of Cationic Bolaamphiphiles: Hydrotropic Counteranions Determine Aggregated Structures. *Chem. Sci.* **2014**, *5*, 3267−3274.
(24) Beyer, H.; Kory, M. J.; Hofer, G.; Stemmer, A.; Schlüter, A. D. Exfoliation of Two-Dimensional Polymer Single Crystals into Thin Sheets and Investigations of Their Surface Structure by High-Resolution Atomic Force Microscopy. *Nanoscale* **2017**, *9*, 9481−9490.
(25) Lei, Z.; Chen, X.; Sun, W.; Zhang, Y.; Wang, Y. Exfoliated Triazine-Based Covalent Organic Nanosheets with Multielectron Redox for High-Performance Lithium Organic Batteries. *Adv. Energy Mater.* **2019**, *9*, 1801010.
(26) Whitesides, G. M.; Grzybowski, B. Self-Assembly at All Scales. *Science* **2002**, *295*, 2418−2421.
(27) Du, F.; Tian, J.; Wang, H.; Liu, B.; Jin, B.; Bai, R. Synthesis and Luminescence of POSS-Containing Perylene Bisimide-Bridged Amphiphilic Polymers. *Macromolecules* **2012**, *45*, 3086−3093.
(28) Li, Z.; Tang, M.; Dai, J.; Wang, T.; Wang, Z.; Bai, W.; Bai, R. Preparation of Covalent Pseudo-Two-Dimensional Polymers in Water by Free Radical Polymerization. *Macromolecules* **2017**, *50*, 4292−4299.
(29) Li, Z.; Tang, M.; Jiang, C.; Bai, R.; Bai, W. Photoinduced Reversible Morphological Transformation of Azobenzene-Containing Pseudo-2D Polymers. *Macromol. Rapid Commun.* **2018**, *39*, 1700880.
(30) Zhuang, X.; Mai, Y.; Wu, D.; Zhang, F.; Feng, X. Two-Dimensional Soft Nanomaterials: A Fascinating World of Materials. *Adv. Mater.* **2015**, *27*, 403−427.
(31) Fuhrhop, J.-H.; Wang, T. Bolaamphiphiles. *Chem. Rev.* **2004**, *104*, 2901−2938.
(32) Nuraje, N.; Bai, H.; Su, K. Bolaamphiphilic Molecules: Assembly and Applications. *Prog. Polym. Sci.* **2013**, *38*, 302−343.
(33) Fyles, T. M. How Do Amphiphiles Form Ion-Conducting Channels in Membranes? Lessons from Linear Oligoesters. *Acc. Chem. Res.* **2013**, *46*, 2847−2855.
(34) Shimizu, T.; Ding, W.; Kameta, N. Soft-Matter Nanotubes: A Platform for Diverse Functions and Applications. *Chem. Rev.* **2020**, *120*, 2347−2407.
(35) Song, B.; Liu, G.; Xu, R.; Yin, S.; Wang, Z.; Zhang, X. Interfacial Self-Organization of Bolaamphiphiles Bearing Mesogenic Groups: Relationships between the Molecular Structures and Their Self-Organized Morphologies. *Langmuir* **2008**, *24*, 3734−3739.
(36) Zhang, N.; Wang, T.; Wu, X.; Jiang, C.; Zhang, T.; Jin, B.; Ji, H.; Bai, W.; Bai, R. From 1D Polymers to 2D Polymers: Preparation of Free-Standing Single-Monomer-Thick Two-Dimensional Conjugated Polymers in Water. *ACS Nano* **2017**, *11*, 7223−7229.
(37) Baek, K.; Yun, G.; Kim, Y.; Kim, D.; Hota, R.; Hwang, I.; Xu, D.; Ko, Y. H.; Gu, G. H.; Suh, J. H. Free-Standing, Single-Monomer-Thick Two-Dimensional Polymers through Covalent Self-Assembly in Solution. *J. Am. Chem. Soc.* **2013**, *135*, 6523−6528.
(38) Zhang, N.; Wang, T.; Wu, X.; Jiang, C.; Chen, F.; Bai, W.; Bai, R. Self-Exfoliation of 2D Covalent Organic Frameworks: Morphology Transformation Induced by Solvent Polarity. *RSC Adv.* **2018**, *8*, 3803−3808.
(39) He, X.; Hsiao, M.-S.; Boott, C. E.; Harniman, R. L.; Nazemi, A.; Li, X.; Winnik, M. A.; Manners, I. Two-Dimensional Assemblies from Crystallizable Homopolymers with Charged Termini. *Nat. Mater.* **2017**, *16*, 481−488.
(40) Ma, X.; Zhang, Y.; Zhang, Y.; Peng, C.; Che, Y.; Zhao, J. Stepwise Formation of Photoconductive Nanotubes through a New Top-Down Method. *Adv. Mater.* **2015**, *27*, 7746−7751.
(41) Ishijima, Y.; Okaniwa, M.; Oaki, Y.; Imai, H. Two Exfoliation Approaches for Organic Layered Compounds: Hydrophilic and Hydrophobic Polydiacetylene Nanosheets. *Chem. Sci.* **2017**, *8*, 647−653.
(42) Guo, S.; Matsukawa, K.; Miyata, T.; Okubo, T.; Kuroda, K.; Shimojima, A. Photoinduced Bending of Self-Assembled Azobenzene-Siloxane Hybrid. *J. Am. Chem. Soc.* **2015**, *137*, 15434−15440.
(43) Xu, B.; Liu, Y.; Sun, X.; Hu, J.; Shi, P.; Huang, X. Semifluorinated Synergistic Nonfouling/Fouling-Release Surface. *ACS Appl. Mater. Interfaces* **2017**, *9*, 16517−16523.
(44) Skrovanek, D. J.; Painter, P. C.; Coleman, M. M. Hydrogen-Bonding in Polymers. 2. Infrared Temperature Studies of Nylon-11. *Macromolecules* **1986**, *19*, 699−705.

https://dx.doi.org/10.1021/acsnano.0c09693
ACS Nano 2021, 15, 3152−3160

(45) Wang, F. C.; Feve, M.; Lam, T. M.; Pascault, J. P. FTIR Analysis of Hydrogen Bonding in Amorphous Linear Aromatic Polyurethanes. I. Influence of Temperature. *J. Polym. Sci., Part B: Polym. Phys.* **1994**, *32*, 1305−1313.
(46) Wang, S.; Zhang, Y.; Xia, Y.; Song, B. Polymorphic Transformation Towards Formation of Nanotubes by Self-Assembly of an Achiral Molecule. *Nanoscale* **2015**, *7*, 17848−17854.
(47) Zhang, Y.; Wang, S.; Liu, Y.; Jin, Y.; Xia, Y.; Song, B. Bilayers Directly Scrolling up to Form Nanotubes *via* Self-Assembly of an Achiral Small Molecule. *Nanoscale* **2017**, *9*, 1491−1495.
(48) Li, Q.; Bao, Y.; Wang, H.; Du, F.; Li, Q.; Jin, B.; Bai, R. A Facile and Highly Efficient Strategy for Esterification of Poly(meth) Acrylic Acid with Halogenated Compounds at Room Temperature Promoted by 1, 1, 3, 3-Tetramethylguanidine. *Polym. Chem.* **2013**, *4*, 2891−2897.
(49) Li, Q.; Wang, T.; Ma, C.; Bai, W.; Bai, R. Facile and Highly Efficient Strategy for Synthesis of Functional Polyesters *via* Tetramethyl Guanidine Promoted Polyesterification at Room Temperature. *ACS Macro Lett.* **2014**, *3*, 1161−1164.
(50) Li, Q.; Hu, X.; Bai, R. Synthesis of Photodegradable Polystyrene with Trithiocarbonate as Linkages. *Macromol. Rapid Commun.* **2015**, *36*, 1810−1815.
(51) Mei, S.; Qi, H.; Zhou, T.; Li, C. Y. Precisely Assembled Cyclic Gold Nanoparticle Frames by 2D Polymer Single-Crystal Templating. *Angew. Chem., Int. Ed.* **2017**, *56*, 13645−13649.
(52) Chen, Y.; Wang, Z.; He, Y.; Yoon, Y. J.; Jung, J.; Zhang, G.; Lin, Z. Light-Enabled Reversible Self-Assembly and Tunable Optical Properties of Stable Hairy Nanoparticles. *Proc. Natl. Acad. Sci. U. S. A.* **2018**, *115*, E1391−E1400.
(53) Xu, F.; Zhang, P.; Zhang, J.; Yu, C.; Yan, D.; Mai, Y. Crystallization-Driven Two-Dimensional Self-Assembly of Amphiphilic PCL-*b*-PEO Coated Gold Nanoparticles in Aqueous Solution. *ACS Macro Lett.* **2018**, *7*, 1062−1067.
(54) Chen, Y.; Wang, Z.; Harn, Y. W.; Pan, S.; Li, Z.; Lin, S.; Peng, J.; Zhang, G.; Lin, Z. Resolving Optical and Catalytic Activities in Thermoresponsive Nanoparticles by Permanent Ligation with Temperature-Sensitive Polymers. *Angew. Chem., Int. Ed.* **2019**, *58*, 11910−11917.

https://dx.doi.org/10.1021/acsnano.0c09693
ACS Nano 2021, 15, 3152−3160